



Model-independent evidence for $J/\psi p$ contributions to $\Lambda_b^0 \rightarrow J/\psi p K^-$ decays

The LHCb collaboration[†]

Abstract

The data sample of $\Lambda_b^0 \rightarrow J/\psi p K^-$ decays acquired with the LHCb detector from 7 and 8 TeV pp collisions, corresponding to an integrated luminosity of 3 fb^{-1} , is inspected for the presence of $J/\psi p$ or $J/\psi K^-$ contributions with minimal assumptions about $K^- p$ contributions. It is demonstrated at more than 9 standard deviations that $\Lambda_b^0 \rightarrow J/\psi p K^-$ decays cannot be described with $K^- p$ contributions alone, and that $J/\psi p$ contributions play a dominant role in this incompatibility. These model-independent results support the previously obtained model-dependent evidence for $P_c^+ \rightarrow J/\psi p$ charmonium-pentaquark states in the same data sample.

Submitted to Physical Review Letters

© CERN on behalf of the LHCb collaboration, license CC-BY-4.0.

[†]Authors are listed at the end of this paper.

From the birth of the quark model, it has been anticipated that baryons could be constructed not only from three quarks, but also from four quarks and an antiquark [1,2], hereafter referred to as pentaquarks. The distribution of $J/\psi p$ mass ($m_{J/\psi p}$) in $\Lambda_b^0 \rightarrow J/\psi p K^-$, $J/\psi \rightarrow \mu^+ \mu^-$ decays observed with the LHCb detector at the LHC shows a narrow peak suggestive of $uudc\bar{c}$ pentaquark formation, amidst the dominant formation of various excitations of the Λ [uds] baryon (Λ^*) decaying to $K^- p$ [3]. (The inclusion of charge conjugate states is implied in this Letter.) Amplitude analyses were performed on all relevant masses and decay angles of the six-dimensional (6D) data, using the helicity formalism and Breit-Wigner amplitudes to describe all resonances. In addition to the previously well established Λ^* resonances, two pentaquark resonances $P_c(4380)^+$ (9σ significance) and $P_c(4450)^+$ (12σ) were required in the model for a good description of the data. The mass, width and fit fractions were determined to be $4380 \pm 8 \pm 29$ MeV, $205 \pm 18 \pm 86$ MeV, $(8.4 \pm 0.7 \pm 4.3)\%$, and $4450 \pm 2 \pm 3$ MeV, $39 \pm 5 \pm 19$ MeV, $(4.1 \pm 0.5 \pm 1.1)\%$, respectively.

The addition of further Λ^* states beyond the well-established ones, and of nonresonant contributions, did not remove the need for two pentaquark states in the model to describe the data. Yet Λ^* spectroscopy is a complex problem, as pointed out in a recent reanalysis of $\bar{K}N$ scattering data [4], in which the well-established $\Lambda(1800)$ state was not seen, and evidence for a few previously unidentified states was obtained. Theoretical models of Λ^* baryons [5–10] predict a much larger number of higher mass excitations than is established experimentally [11]. The high density of predicted states, presumably with large widths, would make it difficult to identify them experimentally. Nonresonant contributions with non-trivial $K^- p$ mass-dependence may also be present. Therefore, it is worth inspecting the $\Lambda_b^0 \rightarrow J/\psi p K^-$ data with an approach that is model-independent with respect to $K^- p$ contributions. Such a method was introduced by the BaBar collaboration [12] and later improved upon by the LHCb collaboration [13]. There it was used to examine $B^0 \rightarrow \psi(2S)\pi^+ K^-$ decays, which are dominated by kaon excitations decaying to $K^- \pi^+$, in order to understand whether the data require the presence of the tetraquark candidate decay, $Z(4430)^+ \rightarrow \psi(2S)\pi^+$. In this Letter, this method is applied to the same $\Lambda_b^0 \rightarrow J/\psi p K^-$ sample previously analyzed in the amplitude analysis [3]. The sensitivity of the model-independent approach to exotic resonances is investigated with simulation studies.

The LHCb detector is a single-arm forward spectrometer covering the pseudorapidity range $2 < \eta < 5$, described in detail in Ref. [14]. The data selection is described in Ref. [3]. A mass window of $\pm 2\sigma$ ($\sigma = 7.5$ MeV) around the Λ_b^0 mass peak is selected, leaving $n_{\text{cand}}^{\text{sig}} = 27\,469$ Λ_b^0 candidates for further analysis, with background fraction (β) equal to 5.4%. The background is subtracted using $n_{\text{cand}}^{\text{side}} = 10\,259$ candidates from the Λ_b^0 sidebands, which extend from ± 38 to ± 140 MeV from the peak (see the supplemental material).

The aim of this analysis is to assess the level of consistency of the data with the hypothesis that all $\Lambda_b^0 \rightarrow J/\psi p K^-$ decays proceed via $\Lambda_b^0 \rightarrow J/\psi \Lambda^*$, $\Lambda^* \rightarrow p K^-$, with minimal assumptions about the spin and lineshape of possible Λ^* contributions. This will be referred to as the null-hypothesis H_0 . Here, Λ^* denotes not only excitations of the Λ baryon, but also nonresonant $K^- p$ contributions or excitations of the Σ baryon. The latter contributions are expected to be small [15]. The analysis method is two-dimensional

and uses the information contained in the Dalitz variables, $(m_{Kp}^2, m_{J/\psi p}^2)$, or equivalently in $(m_{Kp}, \cos \theta_{\Lambda^*})$, where θ_{Λ^*} is the helicity angle of the K^-p system, defined as the angle between the \vec{p}_K and $-\vec{p}_{\Lambda_b^0}$ (or $-\vec{p}_{J/\psi}$) directions in the K^-p rest frame.

The $(m_{Kp}, \cos \theta_{\Lambda^*})$ plane is particularly suited for implementing constraints stemming from the H_0 hypothesis by expanding the $\cos \theta_{\Lambda^*}$ angular distribution in Legendre polynomials P_l :

$$dN/d \cos \theta_{\Lambda^*} = \sum_{l=0}^{l_{\max}} \langle P_l^U \rangle P_l(\cos \theta_{\Lambda^*}),$$

where N is the efficiency-corrected and background-subtracted signal yield, and $\langle P_l^U \rangle$ is an unnormalized Legendre moment of rank l ,

$$\langle P_l^U \rangle = \int_{-1}^{+1} d \cos \theta_{\Lambda^*} P_l(\cos \theta_{\Lambda^*}) dN/d \cos \theta_{\Lambda^*}.$$

Under the H_0 hypothesis, K^-p components cannot contribute to moments of rank higher than $2 J_{\max}$, where J_{\max} is the highest spin of any K^-p contribution at the given m_{Kp} value. This requirement sets the appropriate l_{\max} value, which can be deduced from the lightest experimentally known Λ^* resonances for each J , or from the quark model, as in Fig. 1. An $l_{\max}(m_{Kp})$ function is formed, guided by the values of resonance masses (M_0) lowered by two units of their widths (Γ_0): $l_{\max} = 3$ for m_{Kp} up to 1.64 GeV, 5 up to 1.70 GeV, 7 up to 2.05 GeV and 9 for higher masses as visualized in Fig. 1.

Reflections from other channels, $\Lambda_b^0 \rightarrow P_c^+ K^-$, $P_c^+ \rightarrow J/\psi p$ or $\Lambda_b^0 \rightarrow Z_c^- p$, $Z_c^- \rightarrow J/\psi K^-$, would introduce both low and high rank moments (see the supplemental material for an illustration). The narrower the resonance, the narrower the reflection and the higher the rank l of Legendre polynomials required to describe such a structure.

Selection criteria and backgrounds can also produce high- l structures in the $\cos \theta_{\Lambda^*}$ distribution. Therefore, the data are efficiency-corrected and the background is subtracted. Even though testing the H_0 hypothesis involves only two dimensions, the selection efficiency has some dependence on the other phase-space dimensions, namely the Λ_b^0 and J/ψ helicity angles, as well as angles between the Λ_b^0 decay plane and the J/ψ and Λ^* decay planes. Averaging the efficiency over these additional dimensions (Ω_a) would introduce biases dependent on the exact dynamics of the Λ^* decays. Therefore, a six-dimensional efficiency correction is used. The efficiency parameterization, $\epsilon(m_{Kp}, \cos \theta_{\Lambda^*}, \Omega_a)$, is the same as that used in the amplitude analysis and is described in Sec. 5 of the supplement of Ref. [3].

In order to make the analysis as model-independent as possible, no interpretations are imposed on the m_{Kp} distribution. Instead, the observed efficiency-corrected and background-subtracted histogram of m_{Kp} is used. To obtain a continuous probability density function, $\mathcal{F}(m_{Kp}|H_0)$, a quadratic interpolation of the histogram is performed, as shown in Fig. 2. The essential part of this analysis method is to incorporate the $l \leq l_{\max}(m_{Kp})$ constraint on the Λ^* helicity angle distribution: $\mathcal{F}(m_{Kp}, \cos \theta_{\Lambda^*}|H_0) = \mathcal{F}(m_{Kp}|H_0) \mathcal{F}(\cos \theta_{\Lambda^*}|H_0, m_{Kp})$, where $\mathcal{F}(\cos \theta_{\Lambda^*}|H_0, m_{Kp})$ is obtained via linear interpo-

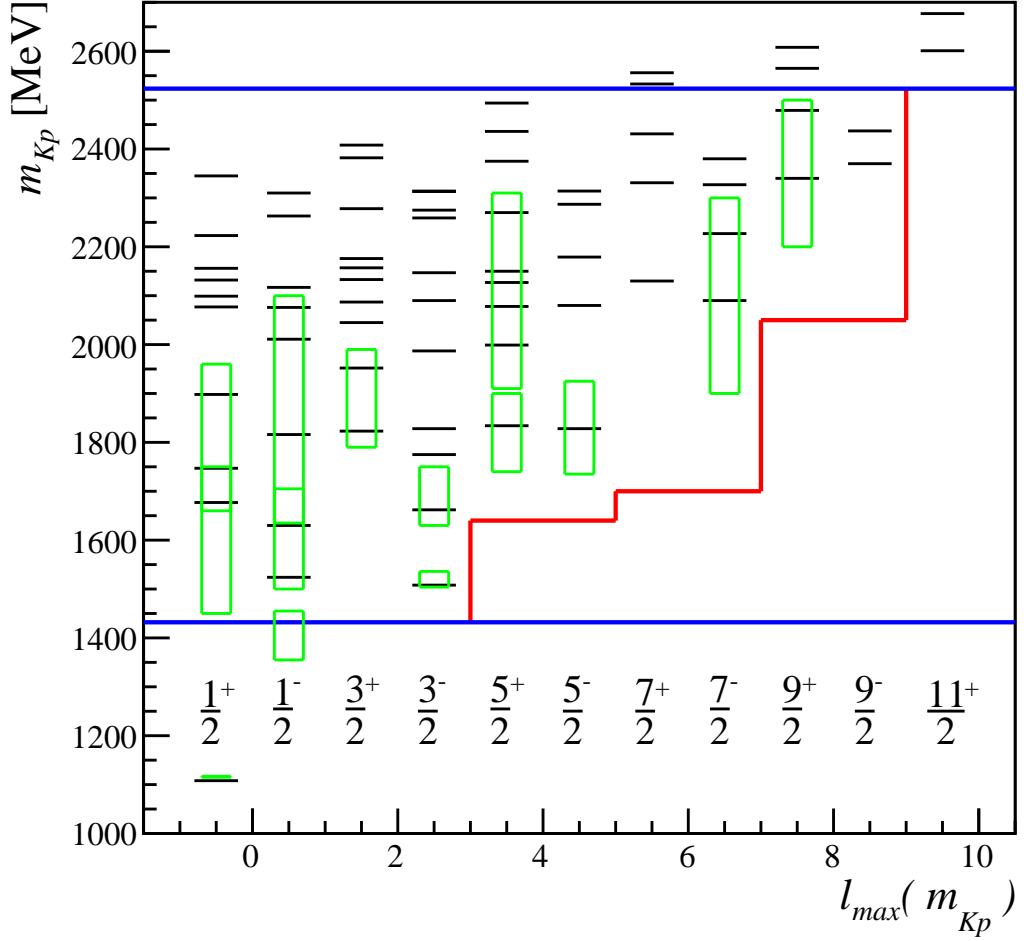


Figure 1: Excitations of the Λ baryon. States predicted in Ref. [7] are shown as short horizontal bars (black) and experimentally well-established Λ^* states are shown as green boxes covering the mass ranges from $M_0 - \Gamma_0$ to $M_0 + \Gamma_0$. The m_{Kp} mass range probed in $\Lambda_b^0 \rightarrow J/\psi p K^-$ decays is shown by long horizontal lines (blue). The $l_{\max}(m_{Kp})$ filter is shown as a stepped line (red). All contributions from Λ^* states with J^P values to the left of the red line are accepted by the filter. The filter works well also for the excitations of the Σ baryon [7, 11] (not shown).

lation between neighboring m_{Kp} bins of

$$\mathcal{F}(\cos \theta_{\Lambda^*} | H_0, m_{Kp}^k) = \sum_{l=0}^{l_{\max}(m_{Kp}^k)} \langle P_l^N \rangle^k P_l(\cos \theta_{\Lambda^*}),$$

where k is the bin index. Here the Legendre moments $\langle P_l^N \rangle^k$ are normalized by the yield in the corresponding m_{Kp} bin, since the overall normalization of $\mathcal{F}(\cos \theta_{\Lambda^*} | H_0, m_{Kp})$ to the data is already contained in the $\mathcal{F}(m_{Kp} | H_0)$ definition. The data are used to determine

$$\langle P_l^U \rangle^k = \sum_{i=1}^{n_{\text{cand}}^k} (w_i / \epsilon_i) P_l(\cos \theta_{\Lambda^*}^i).$$

Here the index i runs over selected $J/\psi p K^-$ candidates in the signal and sideband regions for the k^{th} bin of m_{Kp} (n_{cand}^k is their total number), $\epsilon_i = \epsilon(m_{Kp}^i, \cos\theta_{\Lambda^*}^i, \Omega_a^i)$ is the efficiency correction, and w_i is the background subtraction weight, which equals 1 for events in the signal region and $-\beta n_{\text{cand}}^{\text{sig}}/n_{\text{cand}}^{\text{side}}$ for events in the sideband region. Values of $\langle P_l^U \rangle^k$ are shown in Fig. 3.

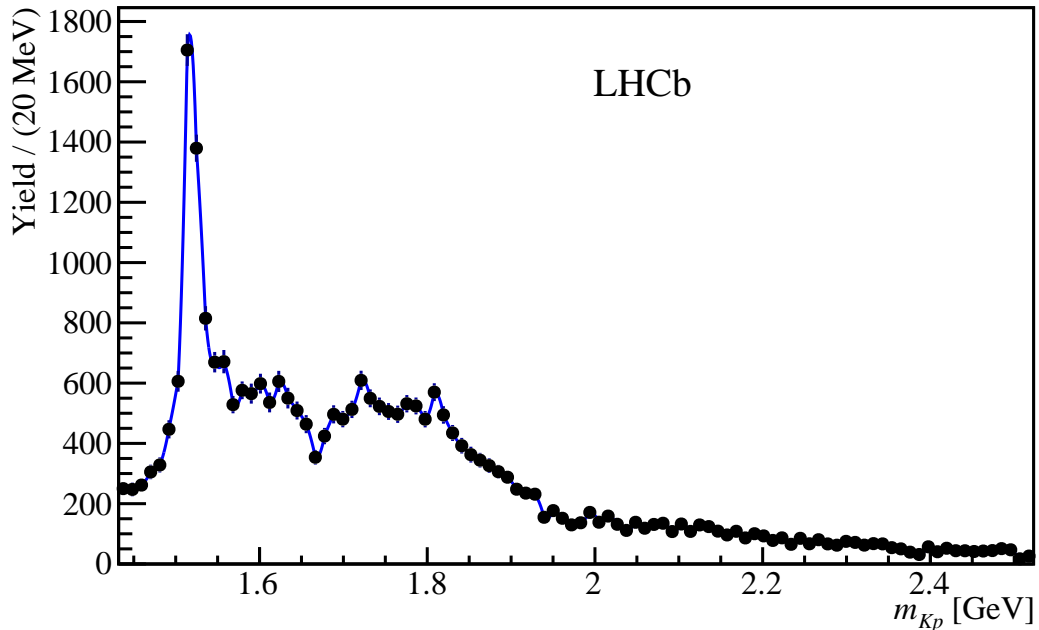


Figure 2: Efficiency-corrected and background-subtracted m_{Kp} distribution of the data (black points with error bars), with $\mathcal{F}(m_{Kp}|H_0)$ superimposed (solid blue line). $\mathcal{F}(m_{Kp}|H_0)$ fits the data by construction.

Instead of using the two-dimensional (2D) distribution of $(m_{Kp}, \cos\theta_{\Lambda^*})$ to evaluate the consistency of the data with the H_0 hypothesis, now expressed by the $l \leq l_{\text{max}}(m_{Kp})$ requirement, it is more convenient to use the $m_{J/\psi p}$ ($m_{J/\psi K}$) distribution, as any deviations from H_0 should appear in the mass region of potential pentaquark (tetraquark) resonances. The projection of $\mathcal{F}(m_{Kp}, \cos\theta_{\Lambda^*}|H_0)$ onto $m_{J/\psi p}$ involves replacing $\cos\theta_{\Lambda^*}$ with $m_{J/\psi p}$ and integrating over m_{Kp} . This integration is carried out numerically, by generating large numbers of simulated events uniformly distributed in m_{Kp} and $\cos\theta_{\Lambda^*}$, calculating the corresponding value of $m_{J/\psi p}$, and then filling a histogram with $\mathcal{F}(m_{Kp}, \cos\theta_{\Lambda^*}|H_0)$ as a weight. In Fig. 4, $\mathcal{F}(m_{J/\psi p}|H_0)$ is compared to the directly obtained efficiency-corrected and background-subtracted $m_{J/\psi p}$ distribution in the data.

To probe the compatibility of $\mathcal{F}(m_{J/\psi p}|H_0)$ with the data, a sensitive test can be constructed by making a specific alternative hypothesis (H_1). Following the method discussed in Ref. [13] H_1 is defined as $l \leq l_{\text{large}}$, where l_{large} is not dependent on m_{Kp} and large enough to reproduce structures induced by $J/\psi p$ or $J/\psi K$ contributions. The significance of the $l_{\text{max}}(m_{Kp}) \leq l \leq l_{\text{large}}$ Legendre moments is probed using the likelihood

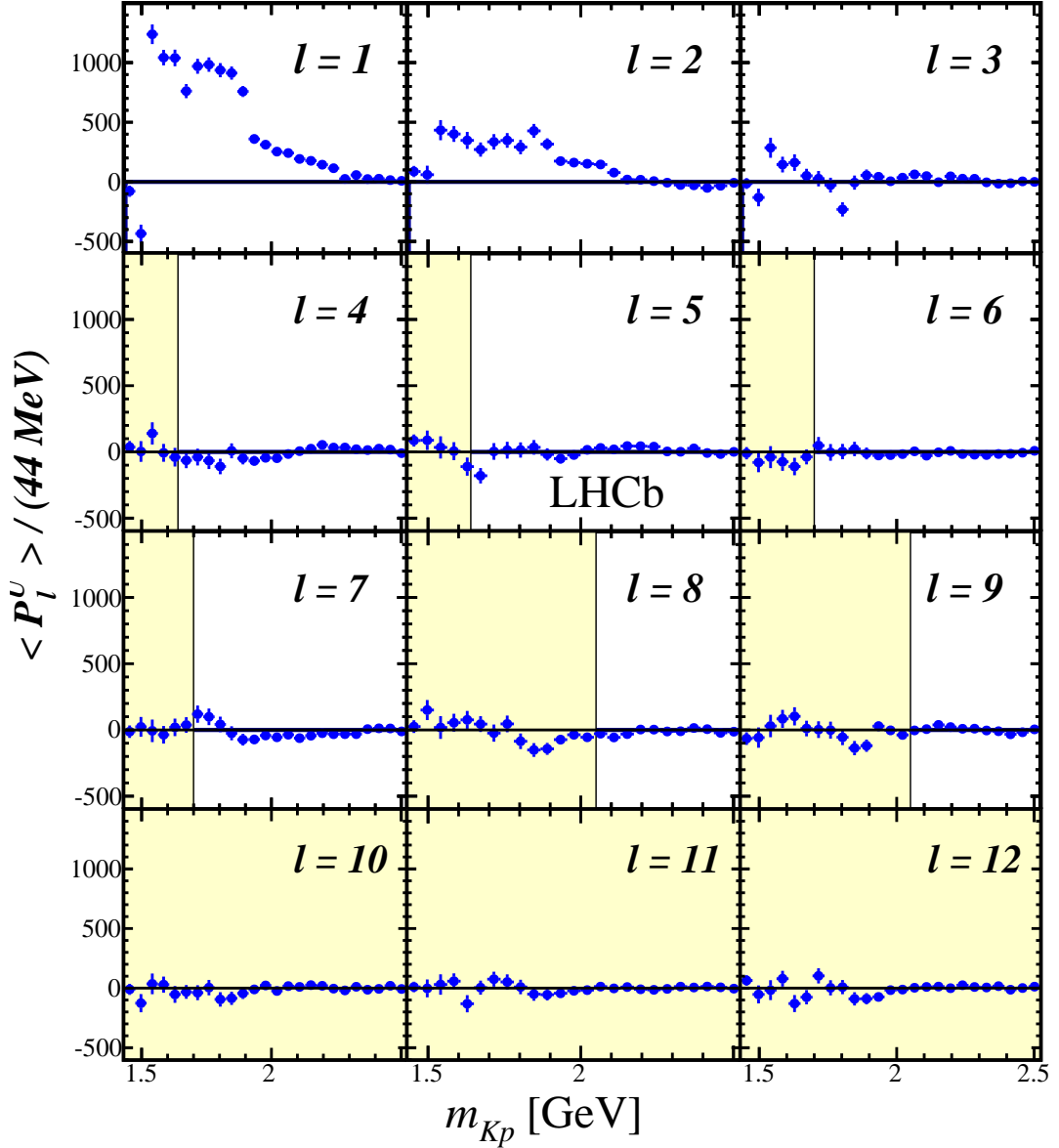


Figure 3: Legendre moments of $\cos \theta_{\Lambda^*}$ as a function of m_{Kp} in the data. Regions excluded by the $l \leq l_{\text{max}}(m_{Kp})$ filter are shaded.

ratio test:

$$\Delta(-2 \ln L) = \sum_{i=1}^{n_{\text{cand}}^{\text{sig}} + n_{\text{cand}}^{\text{side}}} w_i \ln \frac{\mathcal{F}(m_{J/\psi p^i} | H_0) / I_{H_0}}{\mathcal{F}(m_{J/\psi p^i} | H_1) / I_{H_1}},$$

with normalizations $I_{H_{0,1}}$ determined via Monte Carlo integration. Note that the explicit event-by-event efficiency factor cancels in the likelihood ratio, but enters the likelihood normalizations. In order for the test to have optimal sensitivity, the value l_{large} should be set such that the statistically significant features of the data are properly described.

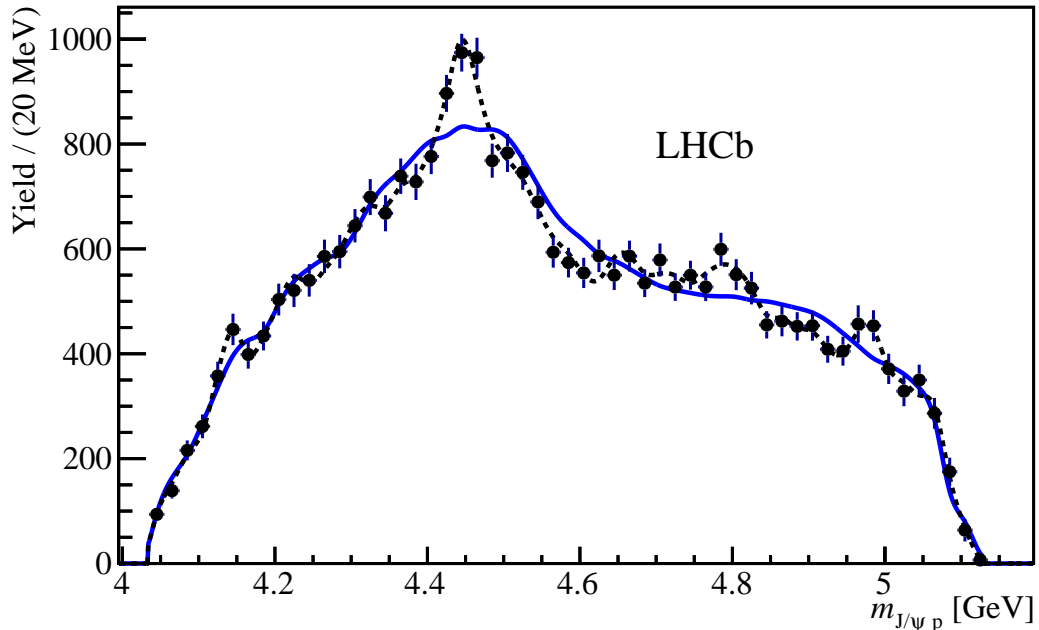


Figure 4: Efficiency-corrected and background-subtracted $m_{J/\psi p}$ distribution of the data (black points with error bars), with $\mathcal{F}(m_{J/\psi p}|H_0)$ (solid blue line) and $\mathcal{F}(m_{J/\psi p}|H_1)$ (dashed black line) superimposed.

Beyond that the power of the test deteriorates. The limit $l_{\text{large}} \rightarrow \infty$ would result in a perfect description of the data, but a weak test since then the test statistic would pick up the fluctuations in the data. For the same reason it is also important to choose l_{large} independently of the actual data. Here $l_{\text{large}} = 31$ is taken, one unit larger than the value used in the model-independent analysis of $B^0 \rightarrow \psi(2S)\pi^+K^-$ [13], as baryons have half-integer spins. The result for $\mathcal{F}(m_{J/\psi p}|H_1)$ is shown in Fig. 4, where it is seen that $l_{\text{large}} = 31$ is sufficient. To make $\mathcal{F}(m_{J/\psi p}|H_{0,1})$ continuous, quadratic splines are used to interpolate between nearby $m_{J/\psi p}$ bins.

The numerical representations of H_0 and of H_1 contain a large number of parameters, requiring extensive statistical simulations to determine the distribution of the test variable for the H_0 hypothesis: $\mathcal{F}_t(\Delta(-2 \ln L)|H_0)$. A large number of pseudoexperiments are generated with $n_{\text{cand}}^{\text{sig}}$ and $n_{\text{cand}}^{\text{side}}$ equal to those obtained in the data. The signal events, contributing a fraction $(1 - \beta)$ to the signal region sample, are generated according to the $\mathcal{F}(m_{Kp}, \cos \theta_{A^*}|H_0)$ function with parameters determined from the data. They are then shaped according to the $\epsilon(m_{Kp}, \cos \theta_{A^*}, \Omega_a)$ function, with the Ω_a angles generated uniformly in phase space. The latter is an approximation, whose possible impact is discussed later. Background events in sideband and signal regions are generated according to the 6D background parameterization previously developed in the amplitude analysis of the same data (Ref. [3] supplement). The pseudoexperiments are subject to the same analysis procedure as the data. The distribution of values of $\Delta(-2 \ln L)$ over more than

10 000 pseudoexperiments determines the form of $\mathcal{F}_t(\Delta(-2 \ln L)|H_0)$, which can then be used to convert the $\Delta(-2 \ln L)$ value obtained from data into a corresponding p -value. A small p -value indicates non- Λ^* contributions in the data. A large p -value means that the data are consistent with the Λ^* -only hypothesis, but does not rule out other contributions.

Before applying this method to the data, it is useful to study its sensitivity with the help of amplitude models. Pseudoexperiments are generated according to the 6D amplitude model containing only Λ^* resonances (the reduced model in Table 1 of Ref. [3]), along with efficiency effects. The distribution of $\Delta(-2 \ln L)$ values is close to that expected from $\mathcal{F}_t(\Delta(-2 \ln L)|H_0)$ (black open and red falling hatched histograms in Fig. 5), thus verifying the 2D model-independent procedure on one example of the Λ^* model. They also indicate that the non-uniformities in $\epsilon(\Omega_a)$ are small enough not to significantly bias the $\mathcal{F}_t(\Delta(-2 \ln L)|H_0)$ distribution when approximating the Ω_a probability density via a uniform distribution. To test the sensitivity of the method to an exotic $P_c^+ \rightarrow J/\psi p$ resonance, the amplitude model described in Ref. [3] is used, but with the $P_c(4450)^+$ contribution removed. Generating many pseudoexperiments from this amplitude model produces a distribution of $\Delta(-2 \ln L)$, which is almost indistinguishable from the $\mathcal{F}_t(\Delta(-2 \ln L)|H_0)$ distribution (blue dotted and red falling hatched histograms in Fig. 5), thus predicting that for such a broad $P_c(4380)^+$ resonance ($\Gamma_0 = 205$ MeV) the false H_0 hypothesis is expected to be accepted (type II error), because the $P_c(4380)^+$ contribution inevitably feeds into the numerical representation of H_0 . Simulations are then repeated while reducing the $P_c(4380)^+$ width by subsequent factors of two, showing a dramatic increase in the power of the test (histograms peaking at 60 and 300). Figure 5 also shows the $\Delta(-2 \ln L)$ distribution obtained with the narrow $P_c(4450)^+$ state restored in the amplitude model and $P_c(4380)^+$ at its nominal 205 MeV width (black rising hatched histogram). The separation from $\mathcal{F}_t(\Delta(-2 \ln L)|H_0)$ is smaller than that of the simulation with a $P_c(4380)^+$ of comparable width (51 MeV) due to the smaller $P_c(4450)^+$ fit fraction. Nevertheless, the separation from $\mathcal{F}_t(\Delta(-2 \ln L)|H_0)$ is clear; thus, if this amplitude model is a good representation of the data, the H_0 hypothesis is expected to essentially always be rejected.

The value of the $\Delta(-2 \ln L)$ test variable obtained from the data is significantly above the $\mathcal{F}_t(\Delta(-2 \ln L)|H_0)$ distribution (see the inset of Fig. 5). To estimate a p -value the simulated $\mathcal{F}_t(\Delta(-2 \ln L)|H_0)$ distribution is fitted with a bifurcated Gaussian function (asymmetric widths); the significance of the H_0 rejection is 10.1σ standard deviations.

To test the sensitivity of the result to possible biases from the background subtraction, either the left or the right sideband is exclusively used, and the weakest obtained rejection of H_0 is 9.8σ . As a further check, the sideband subtraction is performed with the *sPlot* technique [16], in which the w_i weights are obtained from the fit to the $m_{J/\psi pK}$ distribution for candidates in the entire fit range. This increases the significance of the H_0 rejection to 10.4σ . Loosening the cut on the boosted decision tree variable discussed in Ref. [3] increases the signal efficiency by 14%, while doubling the background fraction β , and causes the significance of the H_0 rejection to increase to 11.1σ . Replacing the uniform generation of the Ω_a angles in the H_0 pseudoexperiments with that of the amplitude model without the $P_c(4380)^+$ and $P_c(4450)^+$ states, but generating $(m_{Kp}, \cos \theta_{\Lambda^*})$ in the model-independent way, results in a 9.9σ H_0 rejection.

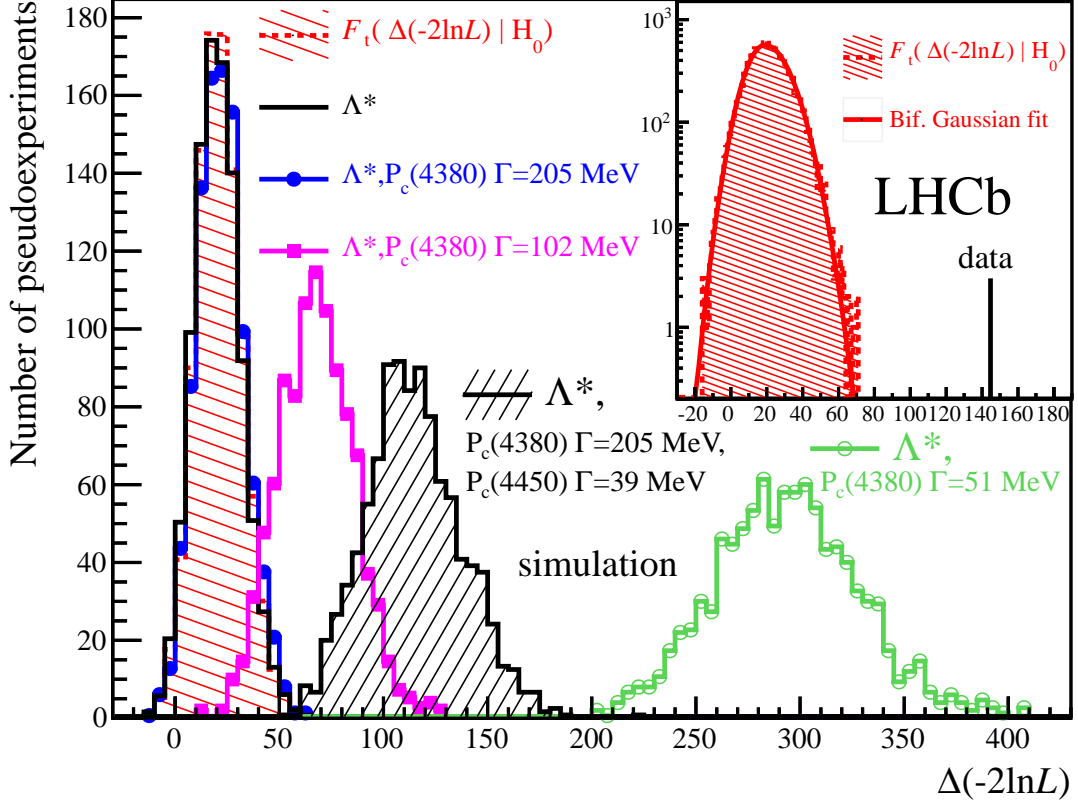


Figure 5: Distributions of $\Delta(-2 \ln L)$ in the model-independent pseudoexperiments corresponding to H_0 (red falling hatched) compared to the distributions for pseudoexperiments generated from various amplitude models and, in the inset, to the bifurcated Gaussian fit function (solid line) and the value obtained for the data (vertical bar).

Figure 4 indicates that the rejection of the H_0 hypothesis has to do with a narrow peak in the data near 4450 MeV. Determination of any P_c^+ parameters is not possible without a model-dependent analysis, because P_c^+ states feed into the numerical representation of H_0 in an intractable manner.

The H_0 testing is repeated using $m_{J/\psi K}$ instead of $m_{J/\psi p}$. The $m_{J/\psi K}$ distribution, with $\mathcal{F}(m_{J/\psi K}|H_0)$ and $\mathcal{F}(m_{J/\psi K}|H_1)$ superimposed, is shown in Fig. 6. The $\Delta(-2 \ln L)$ test gives a 5.3σ rejection of H_0 , which is lower than the rejection obtained using $m_{J/\psi p}$, thus providing model-independent evidence that non- Λ^* contributions are more likely of the $P_c^+ \rightarrow J/\psi p$ type. Further, in the model-dependent amplitude analysis [3], it was seen that the P_c states reflected into the $m_{J/\psi K}$ distribution in the region in which $\mathcal{F}(m_{J/\psi K}|H_0)$ disagrees with the data.

In summary, it has been demonstrated at more than 9 standard deviations that the $\Lambda_b^0 \rightarrow J/\psi p K^-$ decays cannot all be attributed to $K^- p$ resonant or nonresonant contributions. The analysis requires only minimal assumptions on the mass and spin of the

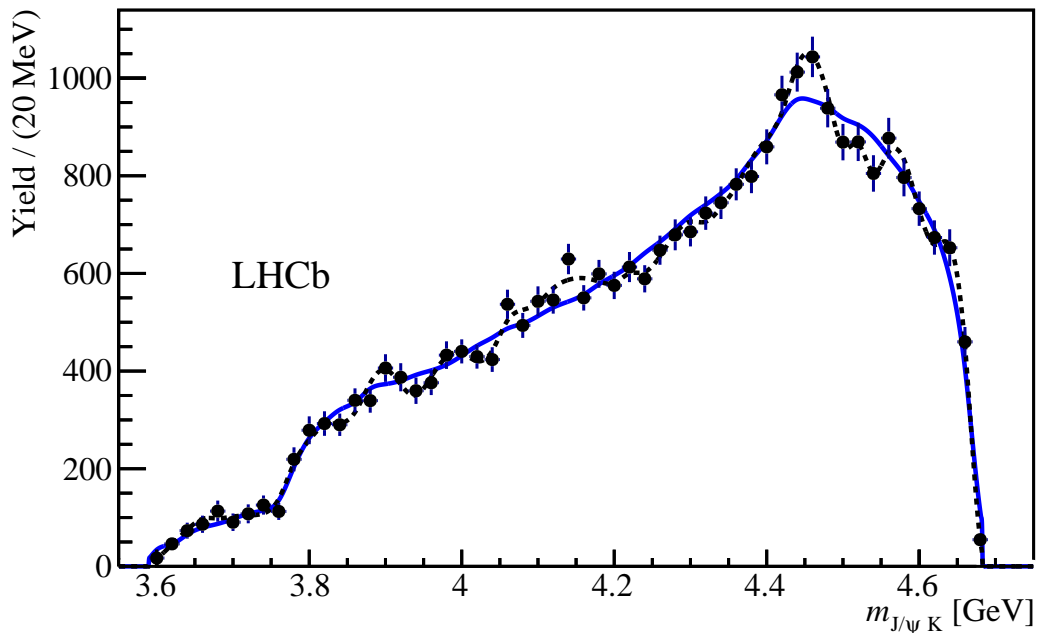


Figure 6: Efficiency-corrected and background-subtracted $m_{J/\psi K}$ distribution of the data (black points with error bars), with $\mathcal{F}(m_{J/\psi K}|H_0)$ (solid blue line) and $\mathcal{F}(m_{J/\psi K}|H_1)$ (dashed black line) superimposed.

K^-p contributions; no assumptions on their number, their resonant or nonresonant nature, or their lineshapes have been made. Non- K^-p contributions, which must be present in the data, can be either of the exotic hadron type, or due to rescattering effects among ordinary hadrons. This result supports the amplitude model-dependent observation of the $J/\psi p$ resonances presented previously [3].

We express our gratitude to our colleagues in the CERN accelerator departments for the excellent performance of the LHC. We thank the technical and administrative staff at the LHCb institutes. We acknowledge support from CERN and from the national agencies: CAPES, CNPq, FAPERJ and FINEP (Brazil); NSFC (China); CNRS/IN2P3 (France); BMBF, DFG and MPG (Germany); INFN (Italy); FOM and NWO (The Netherlands); MNiSW and NCN (Poland); MEN/IFA (Romania); MinES and FANO (Russia); MinECo (Spain); SNSF and SER (Switzerland); NASU (Ukraine); STFC (United Kingdom); NSF (USA). We acknowledge the computing resources that are provided by CERN, IN2P3 (France), KIT and DESY (Germany), INFN (Italy), SURF (The Netherlands), PIC (Spain), GridPP (United Kingdom), RRCKI and Yandex LLC (Russia), CSCS (Switzerland), IFIN-HH (Romania), CBPF (Brazil), PL-GRID (Poland) and OSC (USA). We are indebted to the communities behind the multiple open source software packages on which we depend. Individual groups or members have received support from AvH Foundation (Germany),

EPLANET, Marie Skłodowska-Curie Actions and ERC (European Union), Conseil Général de Haute-Savoie, Labex ENIGMASS and OCEVU, Région Auvergne (France), RFBR and Yandex LLC (Russia), GVA, XuntaGal and GENCAT (Spain), Herchel Smith Fund, The Royal Society, Royal Commission for the Exhibition of 1851 and the Leverhulme Trust (United Kingdom).

References

- [1] M. Gell-Mann, *A schematic model of baryons and mesons*, Phys. Lett. **8** (1964) 214.
- [2] G. Zweig, *An SU_3 model for strong interaction symmetry and its breaking*, CERN-TH-401, 1964.
- [3] LHCb collaboration, R. Aaij *et al.*, *Observation of $J/\psi p$ resonances consistent with pentaquark states in $\Lambda_b^0 \rightarrow J/\psi p K^-$ decays*, Phys. Rev. Lett. **115** (2015) 072001, [arXiv:1507.03414](#).
- [4] C. Fernandez-Ramirez *et al.*, *Coupled-channel model for $\bar{K}N$ scattering in the resonant region*, [arXiv:1510.07065](#).
- [5] R. N. Faustov and V. O. Galkin, *Strange baryon spectroscopy in the relativistic quark model*, Phys. Rev. **D92** (2015) 054005, [arXiv:1507.04530](#).
- [6] S. Capstick and N. Isgur, *Baryons in a relativized quark model with chromodynamics*, Phys. Rev. **D34** (1986) 2809.
- [7] U. Loring, B. C. Metsch, and H. R. Petry, *The light-baryon spectrum in a relativistic quark model with instanton-induced quark forces*, Eur. Phys. J. **A10** (2001) 395, [arXiv:hep-ph/0103289](#).
- [8] T. Melde, W. Plessas, and B. Sengl, *Quark-model identification of baryon ground and resonant states*, Phys. Rev. **D77** (2008) 114002, [arXiv:0806.1454](#).
- [9] E. Santopinto and J. Ferretti, *Strange and nonstrange baryon spectra in the relativistic interacting quark-diquark model with a Gürsey and Radicati-inspired exchange interaction*, Phys. Rev. **C92** (2015) 025202, [arXiv:1412.7571](#).
- [10] G. P. Engel, C. B. Lang, D. Mohler, and A. Schaefer, *QCD with two light dynamical chirally improved quarks: baryons*, Phys. Rev. **D87** (2013) 074504, [arXiv:1301.4318](#).
- [11] Particle Data Group, K. A. Olive *et al.*, *Review of particle physics*, Chin. Phys. **C38** (2014) 090001, and 2015 update.
- [12] BaBar collaboration, B. Aubert *et al.*, *Search for the $Z(4430)^-$ at BaBar*, Phys. Rev. **D79** (2009) 112001, [arXiv:0811.0564](#).

- [13] LHCb collaboration, R. Aaij *et al.*, *A model-independent confirmation of the $Z(4430)^-$ state*, Phys. Rev. **D92** (2015) 112009, [arXiv:1510.01951](#).
- [14] LHCb collaboration, A. A. Alves Jr. *et al.*, *The LHCb detector at the LHC*, JINST **3** (2008) S08005.
- [15] J. F. Donoghue, E. Golowich, W. A. Ponce, and B. R. Holstein, *Analysis of $\Delta S=1$ nonleptonic weak decays and the $\Delta I=1/2$ rule*, Phys. Rev. **D21** (1980) 186.
- [16] M. Pivk and F. R. Le Diberder, *sPlot: A statistical tool to unfold data distributions*, Nucl. Instrum. Meth. **A555** (2005) 356, [arXiv:physics/0402083v3](#).

Appendix: Supplemental material

1 Data sample

The definition of the signal and sideband regions is illustrated in Fig. 7. The background-subtracted and efficiency-corrected distribution of the data on the rectangular Dalitz plane $(m_{Kp}, \cos \theta_{\Lambda^*})$ is shown in Fig. 8.

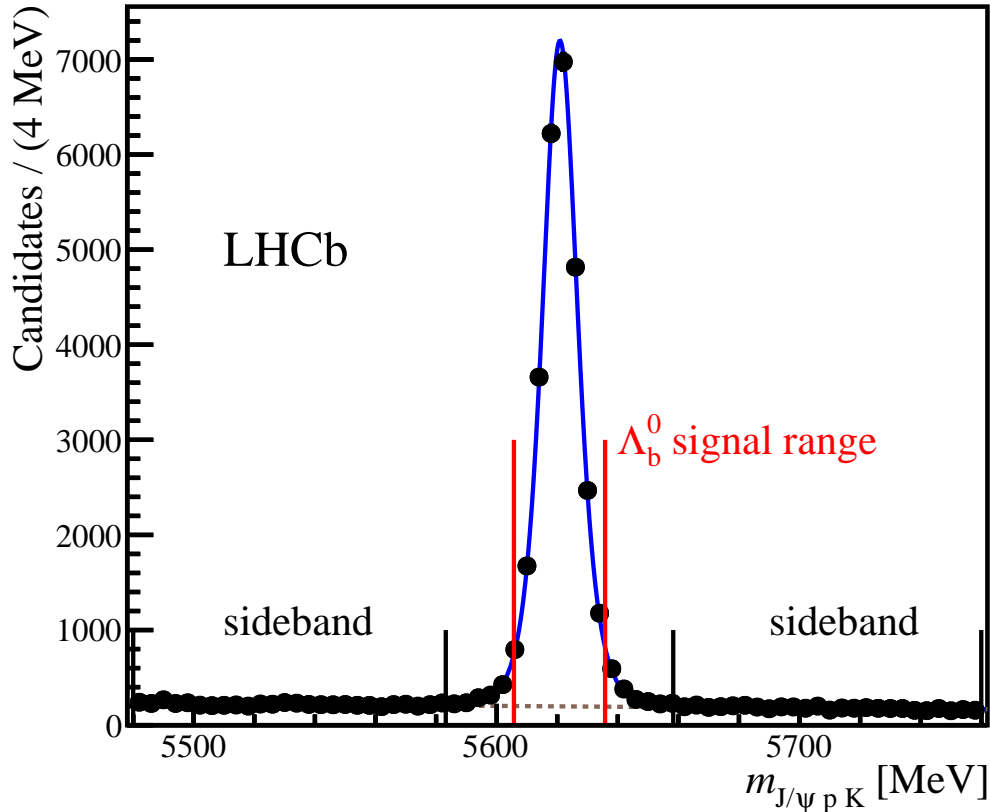


Figure 7: Distribution of $m_{J/\psi p K}$ in the data with the fit of signal and background components superimposed [3]. The fit is used to determine the background fraction β in the $\pm 2\sigma$ signal region around the Λ_b^0 peak (shown by the vertical red bars). The sidebands used in the background subtraction are also shown.

2 Simulations based on amplitude models

The rectangular Dalitz plane $(m_{Kp}, \cos \theta_{\Lambda^*})$ distributions for the large statistics pseudo-samples generated from the amplitude model with only the Λ^* resonances and from the

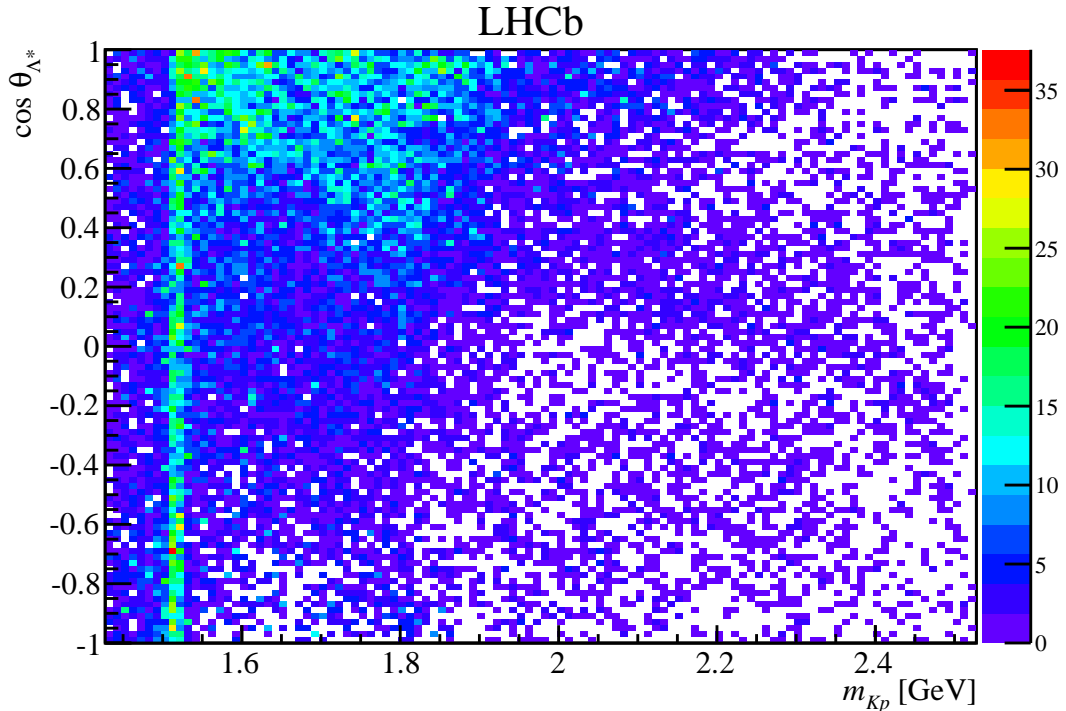


Figure 8: Background-subtracted and efficiency-corrected distribution of the cosine of the Λ^* helicity angle versus m_{Kp} for the data.

amplitude model with only the $P_c(4380)^+$ and $P_c(4450)^+$ resonances are shown in Figs. 9 and 10, respectively. Parameters of the models, without and with the P_c^+ states, were determined by fitting the amplitude models to the data as described in Ref. [3].

The Legendre moments of $\cos\theta_{\Lambda^*}$ distributions ($\langle P_l^U \rangle^k$) in various bins of m_{Kp} are compared between these two simulated pseudo-samples in Fig. 11. The $l \leq l_{\max}(m_{Kp})$ filter, used in forming a numerical representation of the hypothesis that only K^-p contributions are present (H_0), is also illustrated in Fig. 11: moments in the shaded regions ($l > l_{\max}(m_{Kp})$) are neglected. The pentaquark resonances can induce significant values of the moments in these regions, as illustrated with the example amplitude model containing only P_c^+ states. The P_c^+ states also contribute significantly to the unshaded $l \leq l_{\max}(m_{Kp})$ regions, thus feeding into the numerical representation of the H_0 hypothesis, and decreasing the sensitivity of the model-independent approach to exotic hadron contributions. This is especially true for wide resonances, which contribute very little to high moments, as illustrated for the $P_c(4380)^+$ state in Fig. 12. The example amplitude model with only Λ^* resonances contributes to the unshaded regions only, as expected.

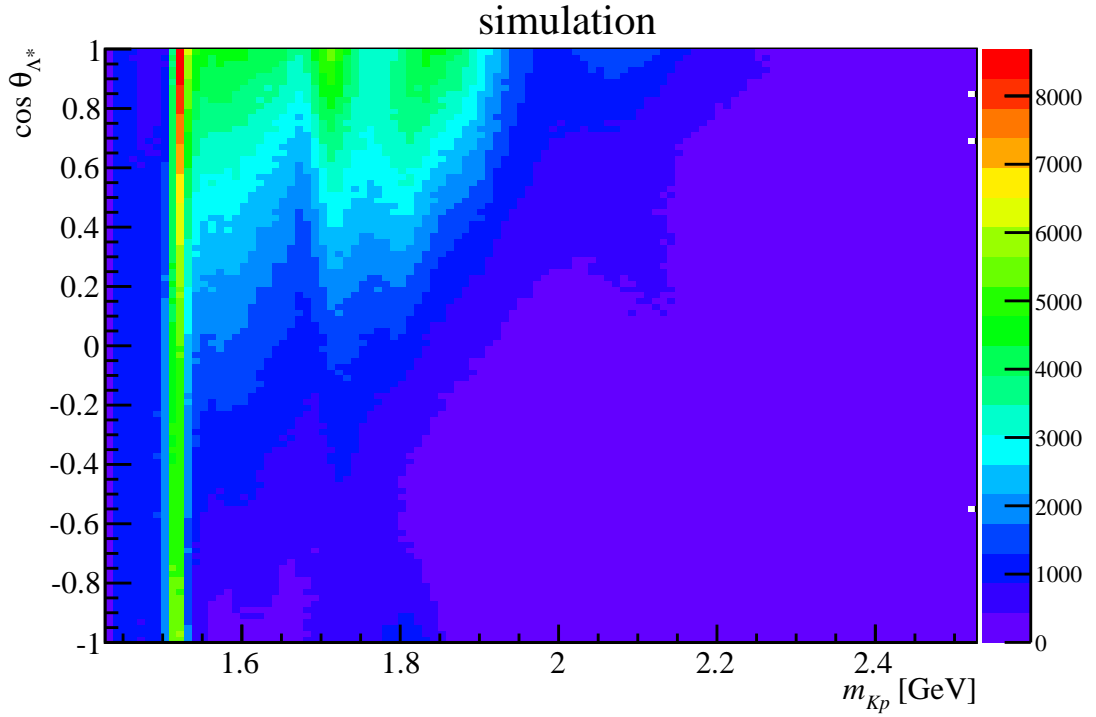


Figure 9: Distribution in a pseudoexperiment of the cosine of the Λ^* helicity angle versus m_{Kp} for the amplitude model with Λ^* resonances only.

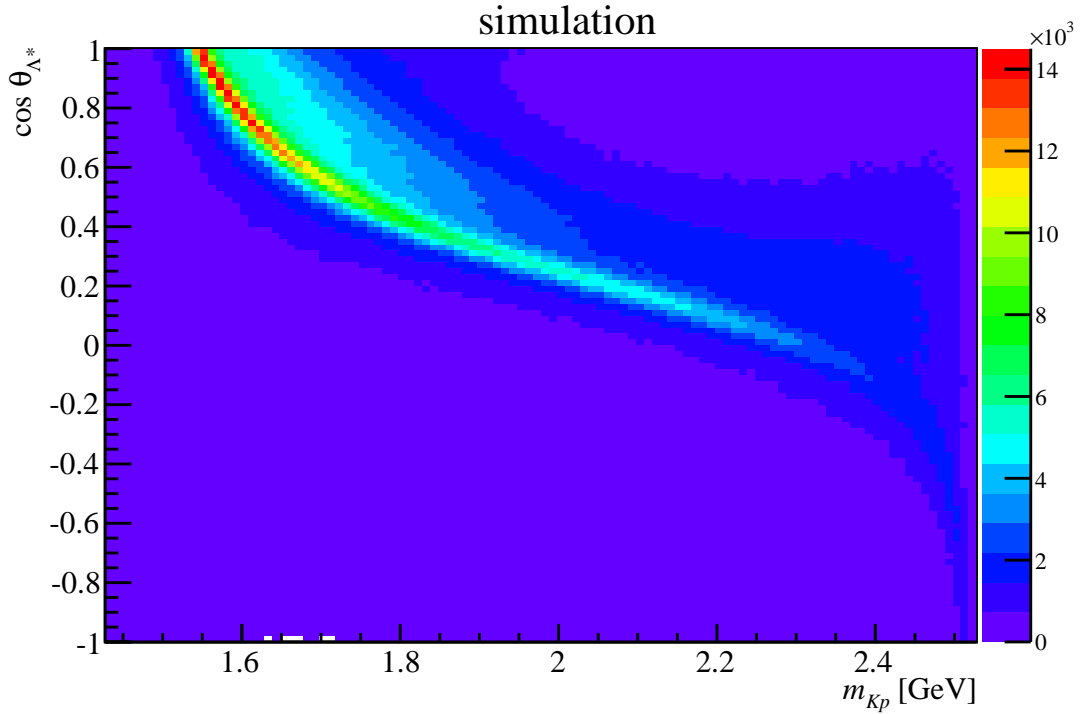


Figure 10: Distribution in a pseudoexperiment of the cosine of the Λ^* helicity angle versus m_{Kp} for the amplitude model with the $P_c(4380)^+$ and $P_c(4450)^+$ resonances only.

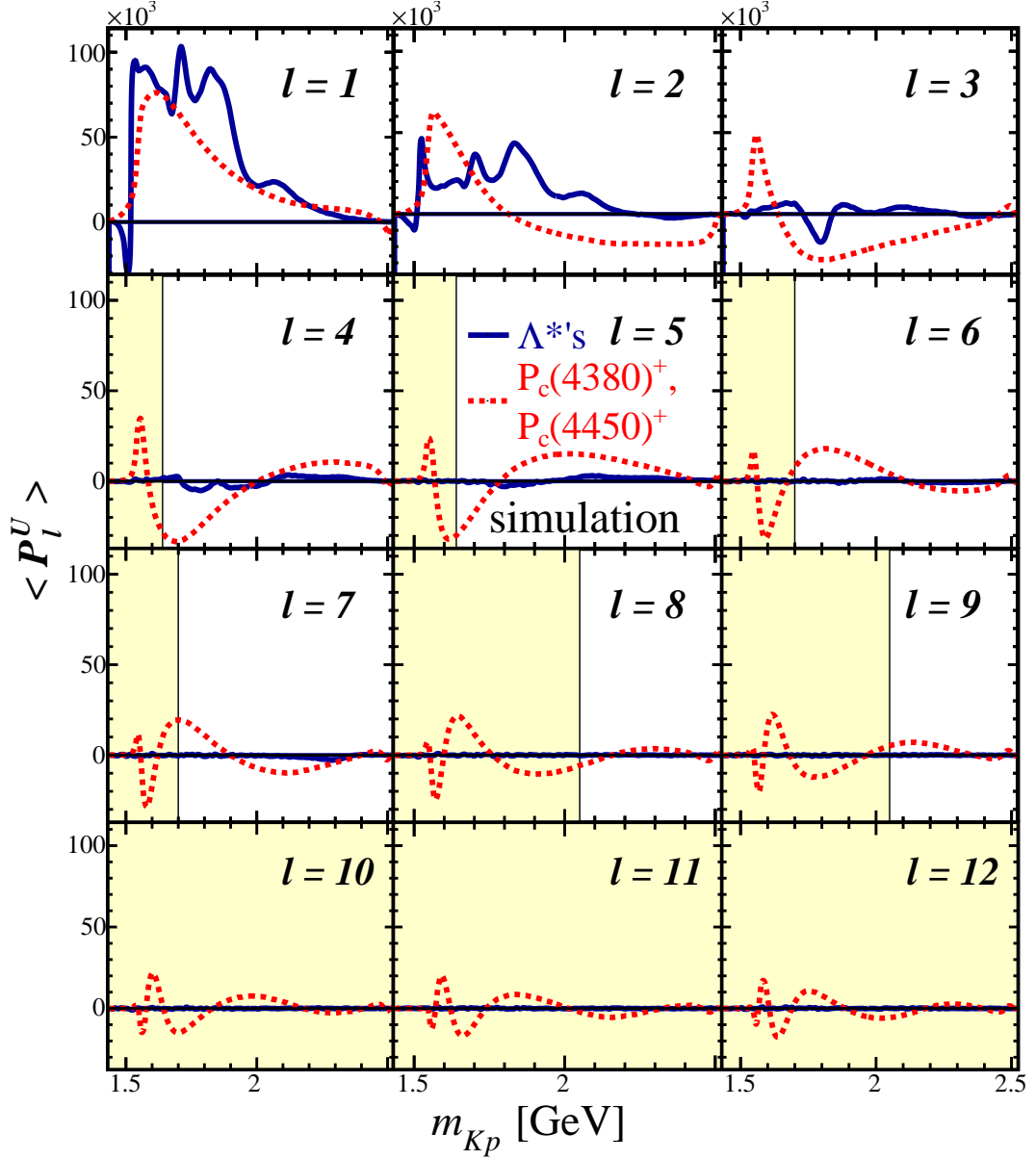


Figure 11: Legendre moments of $\cos\theta_{\Lambda^*}$ as a function of m_{Kp} for the simulated data from the amplitude models with only Λ^* (solid blue lines) and with only $P_c(4380)^+$, $P_c(4450)^+$ contributions (dashed red lines), scaled by 0.5. The regions excluded by the $l \leq l_{\max}(m_{Kp})$ filter are shaded.

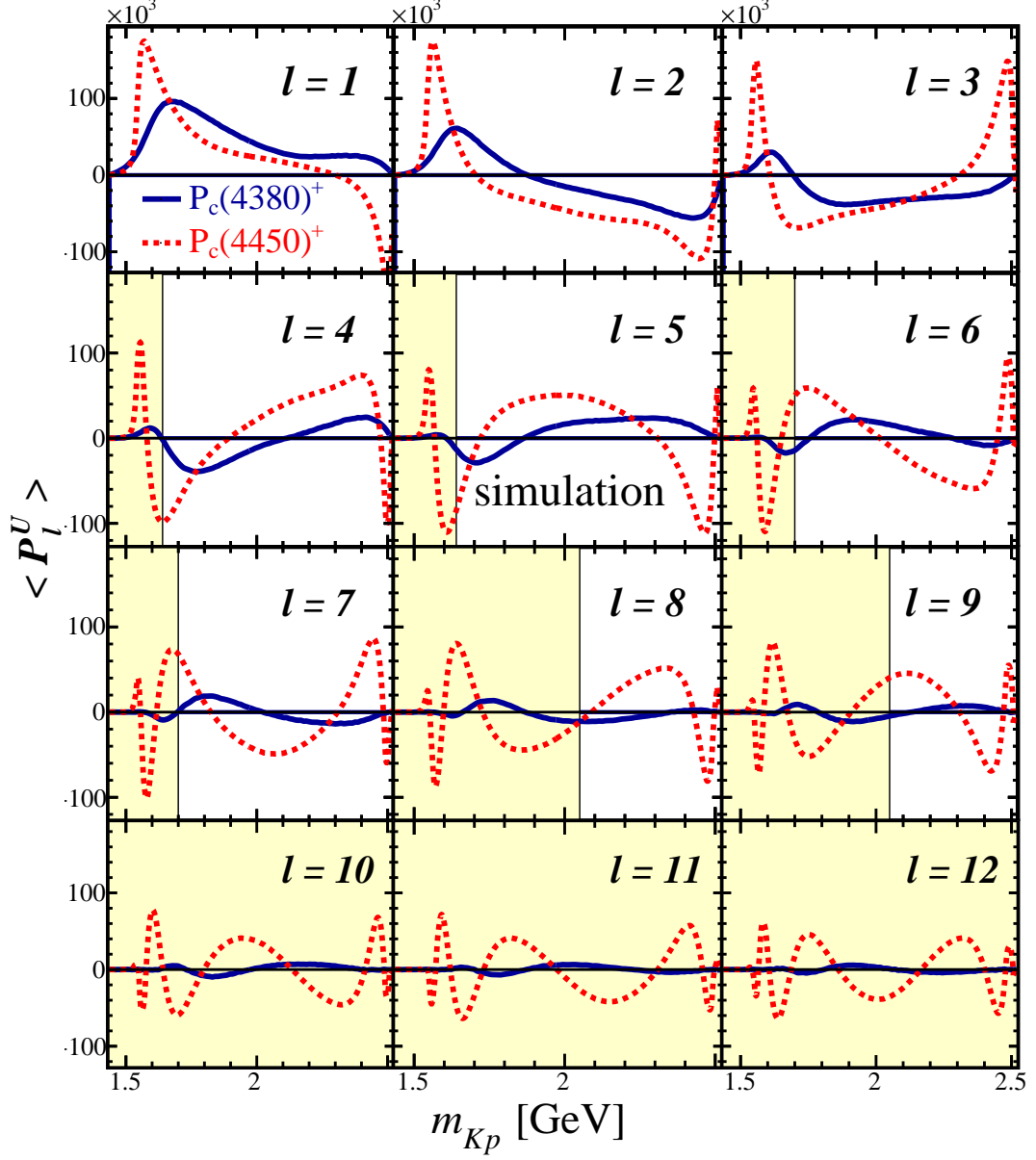


Figure 12: Legendre moments of $\cos\theta_{\Lambda^*}$ as a function of m_{Kp} for the simulated data from amplitude models with only $P_c(4380)^+$ (solid blue lines) and only $P_c(4450)^+$ contributions (dashed red line).

LHCb collaboration

R. Aaij³⁹, C. Abellán Beteta⁴¹, B. Adeva³⁸, M. Adinolfi⁴⁷, Z. Ajaltouni⁵, S. Akar⁶, J. Albrecht¹⁰, F. Alessio³⁹, M. Alexander⁵², S. Ali⁴², G. Alkhazov³¹, P. Alvarez Cartelle⁵⁴, A.A. Alves Jr⁵⁸, S. Amato², S. Amerio²³, Y. Amhis⁷, L. An^{3,40}, L. Anderlini¹⁸, G. Andreassi⁴⁰, M. Andreotti^{17,g}, J.E. Andrews⁵⁹, R.B. Appleby⁵⁵, O. Aquines Gutierrez¹¹, F. Archilli³⁹, P. d'Argent¹², A. Artamonov³⁶, M. Artuso⁶⁰, E. Aslanides⁶, G. Auriemma^{26,n}, M. Baalouch⁵, S. Bachmann¹², J.J. Back⁴⁹, A. Badalov³⁷, C. Baesso⁶¹, S. Baker⁵⁴, W. Baldini¹⁷, R.J. Barlow⁵⁵, C. Barschel³⁹, S. Barsuk⁷, W. Barter³⁹, V. Batozskaya²⁹, V. Battista⁴⁰, A. Bay⁴⁰, L. Beaucourt⁴, J. Beddow⁵², F. Bedeschi²⁴, I. Bediaga¹, L.J. Bel⁴², V. Bellec⁴⁰, N. Belloli^{21,k}, I. Belyaev³², E. Ben-Haim⁸, G. Bencivenni¹⁹, S. Benson³⁹, J. Benton⁴⁷, A. Berezhnoy³³, R. Bernet⁴¹, A. Bertolin²³, F. Betti¹⁵, M.-O. Bettler³⁹, M. van Beuzekom⁴², S. Bifani⁴⁶, P. Billoir⁸, T. Bird⁵⁵, A. Birnkraut¹⁰, A. Bizzeti^{18,i}, T. Blake⁴⁹, F. Blanc⁴⁰, J. Blouw¹¹, S. Blusk⁶⁰, V. Bocci²⁶, A. Bondar³⁵, N. Bondar^{31,39}, W. Bonivento¹⁶, A. Borgheresi^{21,k}, S. Borghi⁵⁵, M. Borisyak⁶⁷, M. Borsato³⁸, M. Boubdir⁹, T.J.V. Bowcock⁵³, E. Bowen⁴¹, C. Bozzi^{17,39}, S. Braun¹², M. Britsch¹², T. Britton⁶⁰, J. Brodzicka⁵⁵, E. Buchanan⁴⁷, C. Burr⁵⁵, A. Bursche², J. Buytaert³⁹, S. Cadeddu¹⁶, R. Calabrese^{17,g}, M. Calvi^{21,k}, M. Calvo Gomez^{37,p}, P. Campana¹⁹, D. Campora Perez³⁹, L. Capriotti⁵⁵, A. Carbone^{15,e}, G. Carboni^{25,l}, R. Cardinale^{20,j}, A. Cardini¹⁶, P. Carniti^{21,k}, L. Carson⁵¹, K. Carvalho Akiba², G. Casse⁵³, L. Cassina^{21,k}, L. Castillo Garcia⁴⁰, M. Cattaneo³⁹, Ch. Cauet¹⁰, G. Cavallero²⁰, R. Cenci^{24,t}, M. Charles⁸, Ph. Charpentier³⁹, G. Chatzikonstantinidis⁴⁶, M. Chefdeville⁴, S. Chen⁵⁵, S.-F. Cheung⁵⁶, V. Chobanova³⁸, M. Chrzaszcz^{41,27}, X. Cid Vidal³⁹, G. Ciezarek⁴², P.E.L. Clarke⁵¹, M. Clemencic³⁹, H.V. Cliff⁴⁸, J. Closier³⁹, V. Coco⁵⁸, J. Cogan⁶, E. Cogneras⁵, V. Cogoni^{16,f}, L. Cojocariu³⁰, G. Collazuol^{23,r}, P. Collins³⁹, A. Comerma-Montells¹², A. Contu³⁹, A. Cook⁴⁷, S. Coquereau⁸, G. Corti³⁹, M. Corvo^{17,g}, B. Couturier³⁹, G.A. Cowan⁵¹, D.C. Craik⁵¹, A. Crocombe⁴⁹, M. Cruz Torres⁶¹, S. Cunliffe⁵⁴, R. Currie⁵⁴, C. D'Ambrosio³⁹, E. Dall'Occo⁴², J. Dalseno⁴⁷, P.N.Y. David⁴², A. Davis⁵⁸, O. De Aguiar Francisco², K. De Bruyn⁶, S. De Capua⁵⁵, M. De Cian¹², J.M. De Miranda¹, L. De Paula², P. De Simone¹⁹, C.-T. Dean⁵², D. Decamp⁴, M. Deckenhoff¹⁰, L. Del Buono⁸, N. Déleage⁴, M. Demmer¹⁰, A. Dendek²⁸, D. Derkach⁶⁷, O. Deschamps⁵, F. Dettori³⁹, B. Dey²², A. Di Canto³⁹, H. Dijkstra³⁹, F. Dordei³⁹, M. Dorigo⁴⁰, A. Dosil Suárez³⁸, A. Dovbnya⁴⁴, K. Dreimanis⁵³, L. Dufour⁴², G. Dujany⁵⁵, K. Dungs³⁹, P. Durante³⁹, R. Dzhelyadin³⁶, A. Dziurda³⁹, A. Dzyuba³¹, S. Easo^{50,39}, U. Egede⁵⁴, V. Egorychev³², S. Eidelman³⁵, S. Eisenhardt⁵¹, U. Eitschberger¹⁰, R. Ekelhof¹⁰, L. Eklund⁵², I. El Rifai⁵, Ch. Elsasser⁴¹, S. Ely⁶⁰, S. Esen¹², H.M. Evans⁴⁸, T. Evans⁵⁶, A. Falabella¹⁵, C. Färber³⁹, N. Farley⁴⁶, S. Farry⁵³, R. Fay⁵³, D. Fazzini^{21,k}, D. Ferguson⁵¹, V. Fernandez Albor³⁸, F. Ferrari^{15,39}, F. Ferreira Rodrigues¹, M. Ferro-Luzzi³⁹, S. Filippov³⁴, M. Fiore^{17,g}, M. Fiorini^{17,g}, M. Firlej²⁸, C. Fitzpatrick⁴⁰, T. Fiutowski²⁸, F. Fleuret^{7,b}, K. Fohl³⁹, M. Fontana¹⁶, F. Fontanelli^{20,j}, D. C. Forshaw⁶⁰, R. Forty³⁹, M. Frank³⁹, C. Frei³⁹, M. Frosini¹⁸, J. Fu²², E. Furfaro^{25,l}, A. Gallas Torreira³⁸, D. Galli^{15,e}, S. Gallorini²³, S. Gambetta⁵¹, M. Gandelman², P. Gandini⁵⁶, Y. Gao³, J. García Pardiñas³⁸, J. Garra Tico⁴⁸, L. Garrido³⁷, P.J. Garsed⁴⁸, D. Gascon³⁷, C. Gaspar³⁹, L. Gavardi¹⁰, G. Gazzoni⁵, D. Gerick¹², E. Gersabeck¹², M. Gersabeck⁵⁵, T. Gershon⁴⁹, Ph. Ghez⁴, S. Gianì⁴⁰, V. Gibson⁴⁸, O.G. Girard⁴⁰, L. Giubega³⁰, V.V. Gligorov⁸, C. Göbel⁶¹, D. Golubkov³², A. Golutvin^{54,39}, A. Gomes^{1,a}, C. Gotti^{21,k}, M. Grabalosa Gándara⁵, R. Graciani Diaz³⁷, L.A. Granado Cardoso³⁹, E. Graugés³⁷, E. Graverini⁴¹, G. Graziani¹⁸, A. Grecu³⁰, P. Griffith⁴⁶, L. Grillo¹², O. Grünberg⁶⁵, E. Gushchin³⁴, Yu. Guz^{36,39}, T. Gys³⁹, T. Hadavizadeh⁵⁶, C. Hadjivasiliou⁶⁰, G. Haefeli⁴⁰,

C. Haen³⁹, S.C. Haines⁴⁸, S. Hall⁵⁴, B. Hamilton⁵⁹, X. Han¹², S. Hansmann-Menzemer¹²,
 N. Harnew⁵⁶, S.T. Harnew⁴⁷, J. Harrison⁵⁵, J. He³⁹, T. Head⁴⁰, A. Heister⁹, K. Hennessy⁵³,
 P. Henrard⁵, L. Henry⁸, J.A. Hernando Morata³⁸, E. van Herwijnen³⁹, M. Heß⁶⁵, A. Hicheur²,
 D. Hill⁵⁶, M. Hoballah⁵, C. Hombach⁵⁵, L. Hongming⁴⁰, W. Hulsbergen⁴², T. Humair⁵⁴,
 M. Hushchyn⁶⁷, N. Hussain⁵⁶, D. Hutchcroft⁵³, M. Idzik²⁸, P. Ilten⁵⁷, R. Jacobsson³⁹,
 A. Jaeger¹², J. Jalocha⁵⁶, E. Jans⁴², A. Jawahery⁵⁹, M. John⁵⁶, D. Johnson³⁹, C.R. Jones⁴⁸,
 C. Joram³⁹, B. Jost³⁹, N. Jurik⁶⁰, S. Kandybei⁴⁴, W. Kanso⁶, M. Karacson³⁹, T.M. Karbach^{39,†},
 S. Karodia⁵², M. Kecke¹², M. Kelsey⁶⁰, I.R. Kenyon⁴⁶, M. Kenzie³⁹, T. Ketel⁴³, E. Khairullin⁶⁷,
 B. Khanji^{21,39,k}, C. Khurewathanakul⁴⁰, T. Kirn⁹, S. Klaver⁵⁵, K. Klimaszewski²⁹, M. Kolpin¹²,
 I. Komarov⁴⁰, R.F. Koopman⁴³, P. Koppenburg⁴², M. Kozeiha⁵, L. Kravchuk³⁴, K. Kreplin¹²,
 M. Kreps⁴⁹, P. Krokovny³⁵, F. Kruse¹⁰, W. Krzemien²⁹, W. Kucewicz^{27,o}, M. Kucharczyk²⁷,
 V. Kudryavtsev³⁵, A. K. Kuonen⁴⁰, K. Kurek²⁹, T. Kvaratskheliya³², D. Lacarrere³⁹,
 G. Lafferty^{55,39}, A. Lai¹⁶, D. Lambert⁵¹, G. Lanfranchi¹⁹, C. Langenbruch⁴⁹, B. Langhans³⁹,
 T. Latham⁴⁹, C. Lazzeroni⁴⁶, R. Le Gac⁶, J. van Leerdam⁴², J.-P. Lees⁴, R. Lefèvre⁵,
 A. Leflat^{33,39}, J. Lefrançois⁷, F. Lemaitre³⁹, E. Lemos Cid³⁸, O. Leroy⁶, T. Lesiak²⁷,
 B. Leverington¹², Y. Li⁷, T. Likhomanenko^{67,66}, R. Lindner³⁹, C. Linn³⁹, F. Lionetto⁴¹,
 B. Liu¹⁶, X. Liu³, D. Loh⁴⁹, I. Longstaff⁵², J.H. Lopes², D. Lucchesi^{23,r}, M. Lucio Martinez³⁸,
 H. Luo⁵¹, A. Lupato²³, E. Luppi^{17,g}, O. Lupton⁵⁶, N. Lusardi²², A. Lusiani²⁴, X. Lyu⁶²,
 F. Machefert⁷, F. Maciuc³⁰, O. Maev³¹, K. Maguire⁵⁵, S. Malde⁵⁶, A. Malinin⁶⁶, G. Manca⁷,
 G. Mancinelli⁶, P. Manning⁶⁰, A. Mapelli³⁹, J. Maratas⁵, J.F. Marchand⁴, U. Marconi¹⁵,
 C. Marin Benito³⁷, P. Marino^{24,t}, J. Marks¹², G. Martellotti²⁶, M. Martin⁶, M. Martinelli⁴⁰,
 D. Martinez Santos³⁸, F. Martinez Vidal⁶⁸, D. Martins Tostes², L.M. Massacrier⁷,
 A. Massafferri¹, R. Matev³⁹, A. Mathad⁴⁹, Z. Mathe³⁹, C. Matteuzzi²¹, A. Mauri⁴¹, B. Maurin⁴⁰,
 A. Mazurov⁴⁶, M. McCann⁵⁴, J. McCarthy⁴⁶, A. McNab⁵⁵, R. McNulty¹³, B. Meadows⁵⁸,
 F. Meier¹⁰, M. Meissner¹², D. Melnychuk²⁹, M. Merk⁴², A. Merli^{22,u}, E. Michielin²³,
 D.A. Milanese⁶⁴, M.-N. Minard⁴, D.S. Mitzel¹², J. Molina Rodriguez⁶¹, I.A. Monroy⁶⁴,
 S. Monteil⁵, M. Morandin²³, P. Morawski²⁸, A. Mordà⁶, M.J. Morello^{24,t}, J. Moron²⁸,
 A.B. Morris⁵¹, R. Mountain⁶⁰, F. Muheim⁵¹, M.M. Mulder⁴², D. Müller⁵⁵, J. Müller¹⁰,
 K. Müller⁴¹, V. Müller¹⁰, M. Mussini¹⁵, B. Muster⁴⁰, P. Naik⁴⁷, T. Nakada⁴⁰, R. Nandakumar⁵⁰,
 A. Nandi⁵⁶, I. Nasteva², M. Needham⁵¹, N. Neri²², S. Neubert¹², N. Neufeld³⁹, M. Neuner¹²,
 A.D. Nguyen⁴⁰, C. Nguyen-Mau^{40,q}, V. Niess⁵, S. Nieswand⁹, R. Niet¹⁰, N. Nikitin³³,
 T. Nikodem¹², A. Novoselov³⁶, D.P. O’Hanlon⁴⁹, A. Oblakowska-Mucha²⁸, V. Obraztsov³⁶,
 S. Ogilvy¹⁹, O. Okhrimenko⁴⁵, R. Oldeman^{16,48,f}, C.J.G. Onderwater⁶⁹, B. Osorio Rodrigues¹,
 J.M. Otalora Goicochea², A. Otto³⁹, P. Owen⁵⁴, A. Oyanguren⁶⁸, A. Palano^{14,d}, F. Palombo^{22,u},
 M. Palutan¹⁹, J. Panman³⁹, A. Papanestis⁵⁰, M. Pappagallo⁵², L.L. Pappalardo^{17,g},
 C. Pappenheimer⁵⁸, W. Parker⁵⁹, C. Parkes⁵⁵, G. Passaleva¹⁸, G.D. Patel⁵³, M. Patel⁵⁴,
 C. Patrignani^{20,j}, A. Pearce^{55,50}, A. Pellegrino⁴², G. Penso^{26,m}, M. Pepe Altarelli³⁹,
 S. Perazzini³⁹, P. Perret⁵, L. Pescatore⁴⁶, K. Petridis⁴⁷, A. Petrolini^{20,j}, M. Petruzzo²²,
 E. Picatoste Olloqui³⁷, B. Pietrzyk⁴, M. Pikies²⁷, D. Pinci²⁶, A. Pistone²⁰, A. Piucci¹²,
 S. Playfer⁵¹, M. Plo Casasus³⁸, T. Poikela³⁹, F. Polci⁸, A. Poluektov^{49,35}, I. Polyakov³²,
 E. Polycarpo², A. Popov³⁶, D. Popov^{11,39}, B. Popovici³⁰, C. Potterat², E. Price⁴⁷, J.D. Price⁵³,
 J. Prisciandaro³⁸, A. Pritchard⁵³, C. Prouve⁴⁷, V. Pugatch⁴⁵, A. Puig Navarro⁴⁰, G. Punzi^{24,s},
 W. Qian⁵⁶, R. Quagliani^{7,47}, B. Rachwal²⁷, J.H. Rademacker⁴⁷, M. Rama²⁴, M. Ramos Pernas³⁸,
 M.S. Rangel², I. Raniuk⁴⁴, G. Raven⁴³, F. Redi⁵⁴, S. Reichert¹⁰, A.C. dos Reis¹, V. Renaudin⁷,
 S. Ricciardi⁵⁰, S. Richards⁴⁷, M. Rihl³⁹, K. Rinnert^{53,39}, V. Rives Molina³⁷, P. Robbe⁷,
 A.B. Rodrigues¹, E. Rodrigues⁵⁸, J.A. Rodriguez Lopez⁶⁴, P. Rodriguez Perez⁵⁵,

A. Rogozhnikov⁶⁷, S. Roiser³⁹, V. Romanovsky³⁶, A. Romero Vidal³⁸, J. W. Ronayne¹³, M. Rotondo²³, T. Ruf³⁹, P. Ruiz Valls⁶⁸, J.J. Saborido Silva³⁸, N. Sagidova³¹, B. Saitta^{16,f}, V. Salustino Guimaraes², C. Sanchez Mayordomo⁶⁸, B. Sanmartin Sedes³⁸, R. Santacesaria²⁶, C. Santamarina Rios³⁸, M. Santimaria¹⁹, E. Santovetti^{25,l}, A. Sarti^{19,m}, C. Satriano^{26,n}, A. Satta²⁵, D.M. Saunders⁴⁷, D. Savrina^{32,33}, S. Schael⁹, M. Schiller³⁹, H. Schindler³⁹, M. Schlupp¹⁰, M. Schmelling¹¹, T. Schmelzer¹⁰, B. Schmidt³⁹, O. Schneider⁴⁰, A. Schopper³⁹, M. Schubiger⁴⁰, M.-H. Schune⁷, R. Schwemmer³⁹, B. Sciascia¹⁹, A. Sciubba^{26,m}, A. Semennikov³², A. Sergi⁴⁶, N. Serra⁴¹, J. Serrano⁶, L. Sestini²³, P. Seyfert²¹, M. Shapkin³⁶, I. Shapoval^{17,44,g}, Y. Shcheglov³¹, T. Shears⁵³, L. Shekhtman³⁵, V. Shevchenko⁶⁶, A. Shires¹⁰, B.G. Siddi¹⁷, R. Silva Coutinho⁴¹, L. Silva de Oliveira², G. Simi^{23,s}, M. Sirendi⁴⁸, N. Skidmore⁴⁷, T. Skwarnicki⁶⁰, E. Smith⁵⁴, I.T. Smith⁵¹, J. Smith⁴⁸, M. Smith⁵⁵, H. Snoek⁴², M.D. Sokoloff⁵⁸, F.J.P. Soler⁵², F. Soomro⁴⁰, D. Souza⁴⁷, B. Souza De Paula², B. Spaan¹⁰, P. Spradlin⁵², S. Sridharan³⁹, F. Stagni³⁹, M. Stahl¹², S. Stahl³⁹, S. Stefkova⁵⁴, O. Steinkamp⁴¹, O. Stenyakin³⁶, S. Stevenson⁵⁶, S. Stoica³⁰, S. Stone⁶⁰, B. Storaci⁴¹, S. Stracka^{24,t}, M. Straticiu³⁰, U. Straumann⁴¹, L. Sun⁵⁸, W. Sutcliffe⁵⁴, K. Swientek²⁸, S. Swientek¹⁰, V. Syropoulos⁴³, M. Szczekowski²⁹, T. Szumlak²⁸, S. T'Jampens⁴, A. Tayduganov⁶, T. Tekampe¹⁰, G. Tellarini^{17,g}, F. Teubert³⁹, C. Thomas⁵⁶, E. Thomas³⁹, J. van Tilburg⁴², V. Tisserand⁴, M. Tobin⁴⁰, S. Tolk⁴³, L. Tomassetti^{17,g}, D. Tonelli³⁹, S. Topp-Joergensen⁵⁶, E. Tournefier⁴, S. Tourneur⁴⁰, K. Trabelsi⁴⁰, M. Traill⁵², M.T. Tran⁴⁰, M. Tresch⁴¹, A. Trisovic³⁹, A. Tsaregorodtsev⁶, P. Tsopelas⁴², N. Tuning^{42,39}, A. Ukleja²⁹, A. Ustyuzhanin^{67,66}, U. Uwer¹², C. Vacca^{16,39,f}, V. Vagnoni^{15,39}, S. Valat³⁹, G. Valenti¹⁵, A. Vallier⁷, R. Vazquez Gomez¹⁹, P. Vazquez Regueiro³⁸, C. Vázquez Sierra³⁸, S. Vecchi¹⁷, M. van Veghel⁴², J.J. Velthuis⁴⁷, M. Veltri^{18,h}, G. Veneziano⁴⁰, M. Vesterinen¹², B. Viaud⁷, D. Vieira², M. Vieites Diaz³⁸, X. Vilasis-Cardona^{37,p}, V. Volkov³³, A. Vollhardt⁴¹, D. Voong⁴⁷, A. Vorobyev³¹, V. Vorobyev³⁵, C. Voß⁶⁵, J.A. de Vries⁴², R. Waldi⁶⁵, C. Wallace⁴⁹, R. Wallace¹³, J. Walsh²⁴, J. Wang⁶⁰, D.R. Ward⁴⁸, N.K. Watson⁴⁶, D. Websdale⁵⁴, A. Weiden⁴¹, M. Whitehead³⁹, J. Wicht⁴⁹, G. Wilkinson^{56,39}, M. Wilkinson⁶⁰, M. Williams³⁹, M.P. Williams⁴⁶, M. Williams⁵⁷, T. Williams⁴⁶, F.F. Wilson⁵⁰, J. Wimberley⁵⁹, J. Wishahi¹⁰, W. Wislicki²⁹, M. Witek²⁷, G. Wormser⁷, S.A. Wotton⁴⁸, K. Wraight⁵², S. Wright⁴⁸, K. Wyllie³⁹, Y. Xie⁶³, Z. Xu⁴⁰, Z. Yang³, H. Yin⁶³, J. Yu⁶³, X. Yuan³⁵, O. Yushchenko³⁶, M. Zangoli¹⁵, M. Zavertyaev^{11,c}, L. Zhang³, Y. Zhang⁷, A. Zhelezov¹², Y. Zheng⁶², A. Zhokhov³², L. Zhong³, V. Zhukov⁹, S. Zucchelli¹⁵.

¹Centro Brasileiro de Pesquisas Físicas (CBPF), Rio de Janeiro, Brazil

²Universidade Federal do Rio de Janeiro (UFRJ), Rio de Janeiro, Brazil

³Center for High Energy Physics, Tsinghua University, Beijing, China

⁴LAPP, Université Savoie Mont-Blanc, CNRS/IN2P3, Annecy-Le-Vieux, France

⁵Clermont Université, Université Blaise Pascal, CNRS/IN2P3, LPC, Clermont-Ferrand, France

⁶CPPM, Aix-Marseille Université, CNRS/IN2P3, Marseille, France

⁷LAL, Université Paris-Sud, CNRS/IN2P3, Orsay, France

⁸LPNHE, Université Pierre et Marie Curie, Université Paris Diderot, CNRS/IN2P3, Paris, France

⁹I. Physikalisches Institut, RWTH Aachen University, Aachen, Germany

¹⁰Fakultät Physik, Technische Universität Dortmund, Dortmund, Germany

¹¹Max-Planck-Institut für Kernphysik (MPIK), Heidelberg, Germany

¹²Physikalisches Institut, Ruprecht-Karls-Universität Heidelberg, Heidelberg, Germany

¹³School of Physics, University College Dublin, Dublin, Ireland

¹⁴Sezione INFN di Bari, Bari, Italy

¹⁵Sezione INFN di Bologna, Bologna, Italy

- ¹⁶ *Sezione INFN di Cagliari, Cagliari, Italy*
- ¹⁷ *Sezione INFN di Ferrara, Ferrara, Italy*
- ¹⁸ *Sezione INFN di Firenze, Firenze, Italy*
- ¹⁹ *Laboratori Nazionali dell'INFN di Frascati, Frascati, Italy*
- ²⁰ *Sezione INFN di Genova, Genova, Italy*
- ²¹ *Sezione INFN di Milano Bicocca, Milano, Italy*
- ²² *Sezione INFN di Milano, Milano, Italy*
- ²³ *Sezione INFN di Padova, Padova, Italy*
- ²⁴ *Sezione INFN di Pisa, Pisa, Italy*
- ²⁵ *Sezione INFN di Roma Tor Vergata, Roma, Italy*
- ²⁶ *Sezione INFN di Roma La Sapienza, Roma, Italy*
- ²⁷ *Henryk Niewodniczanski Institute of Nuclear Physics Polish Academy of Sciences, Kraków, Poland*
- ²⁸ *AGH - University of Science and Technology, Faculty of Physics and Applied Computer Science, Kraków, Poland*
- ²⁹ *National Center for Nuclear Research (NCBJ), Warsaw, Poland*
- ³⁰ *Horia Hulubei National Institute of Physics and Nuclear Engineering, Bucharest-Magurele, Romania*
- ³¹ *Petersburg Nuclear Physics Institute (PNPI), Gatchina, Russia*
- ³² *Institute of Theoretical and Experimental Physics (ITEP), Moscow, Russia*
- ³³ *Institute of Nuclear Physics, Moscow State University (SINP MSU), Moscow, Russia*
- ³⁴ *Institute for Nuclear Research of the Russian Academy of Sciences (INR RAN), Moscow, Russia*
- ³⁵ *Budker Institute of Nuclear Physics (SB RAS) and Novosibirsk State University, Novosibirsk, Russia*
- ³⁶ *Institute for High Energy Physics (IHEP), Protvino, Russia*
- ³⁷ *Universitat de Barcelona, Barcelona, Spain*
- ³⁸ *Universidad de Santiago de Compostela, Santiago de Compostela, Spain*
- ³⁹ *European Organization for Nuclear Research (CERN), Geneva, Switzerland*
- ⁴⁰ *Ecole Polytechnique Fédérale de Lausanne (EPFL), Lausanne, Switzerland*
- ⁴¹ *Physik-Institut, Universität Zürich, Zürich, Switzerland*
- ⁴² *Nikhef National Institute for Subatomic Physics, Amsterdam, The Netherlands*
- ⁴³ *Nikhef National Institute for Subatomic Physics and VU University Amsterdam, Amsterdam, The Netherlands*
- ⁴⁴ *NSC Kharkiv Institute of Physics and Technology (NSC KIPT), Kharkiv, Ukraine*
- ⁴⁵ *Institute for Nuclear Research of the National Academy of Sciences (KINR), Kyiv, Ukraine*
- ⁴⁶ *University of Birmingham, Birmingham, United Kingdom*
- ⁴⁷ *H.H. Wills Physics Laboratory, University of Bristol, Bristol, United Kingdom*
- ⁴⁸ *Cavendish Laboratory, University of Cambridge, Cambridge, United Kingdom*
- ⁴⁹ *Department of Physics, University of Warwick, Coventry, United Kingdom*
- ⁵⁰ *STFC Rutherford Appleton Laboratory, Didcot, United Kingdom*
- ⁵¹ *School of Physics and Astronomy, University of Edinburgh, Edinburgh, United Kingdom*
- ⁵² *School of Physics and Astronomy, University of Glasgow, Glasgow, United Kingdom*
- ⁵³ *Oliver Lodge Laboratory, University of Liverpool, Liverpool, United Kingdom*
- ⁵⁴ *Imperial College London, London, United Kingdom*
- ⁵⁵ *School of Physics and Astronomy, University of Manchester, Manchester, United Kingdom*
- ⁵⁶ *Department of Physics, University of Oxford, Oxford, United Kingdom*
- ⁵⁷ *Massachusetts Institute of Technology, Cambridge, MA, United States*
- ⁵⁸ *University of Cincinnati, Cincinnati, OH, United States*
- ⁵⁹ *University of Maryland, College Park, MD, United States*
- ⁶⁰ *Syracuse University, Syracuse, NY, United States*
- ⁶¹ *Pontifícia Universidade Católica do Rio de Janeiro (PUC-Rio), Rio de Janeiro, Brazil, associated to ²*
- ⁶² *University of Chinese Academy of Sciences, Beijing, China, associated to ³*
- ⁶³ *Institute of Particle Physics, Central China Normal University, Wuhan, Hubei, China, associated to ³*
- ⁶⁴ *Departamento de Física, Universidad Nacional de Colombia, Bogota, Colombia, associated to ⁸*
- ⁶⁵ *Institut für Physik, Universität Rostock, Rostock, Germany, associated to ¹²*

- ⁶⁶ *National Research Centre Kurchatov Institute, Moscow, Russia, associated to* ³²
- ⁶⁷ *Yandex School of Data Analysis, Moscow, Russia, associated to* ³²
- ⁶⁸ *Instituto de Fisica Corpuscular (IFIC), Universitat de Valencia-CSIC, Valencia, Spain, associated to* ³⁷
- ⁶⁹ *Van Swinderen Institute, University of Groningen, Groningen, The Netherlands, associated to* ⁴²
- ^a *Universidade Federal do Triângulo Mineiro (UFMT), Uberaba-MG, Brazil*
- ^b *Laboratoire Leprince-Ringuet, Palaiseau, France*
- ^c *P.N. Lebedev Physical Institute, Russian Academy of Science (LPI RAS), Moscow, Russia*
- ^d *Università di Bari, Bari, Italy*
- ^e *Università di Bologna, Bologna, Italy*
- ^f *Università di Cagliari, Cagliari, Italy*
- ^g *Università di Ferrara, Ferrara, Italy*
- ^h *Università di Urbino, Urbino, Italy*
- ⁱ *Università di Modena e Reggio Emilia, Modena, Italy*
- ^j *Università di Genova, Genova, Italy*
- ^k *Università di Milano Bicocca, Milano, Italy*
- ^l *Università di Roma Tor Vergata, Roma, Italy*
- ^m *Università di Roma La Sapienza, Roma, Italy*
- ⁿ *Università della Basilicata, Potenza, Italy*
- ^o *AGH - University of Science and Technology, Faculty of Computer Science, Electronics and Telecommunications, Kraków, Poland*
- ^p *LIFAELS, La Salle, Universitat Ramon Llull, Barcelona, Spain*
- ^q *Hanoi University of Science, Hanoi, Viet Nam*
- ^r *Università di Padova, Padova, Italy*
- ^s *Università di Pisa, Pisa, Italy*
- ^t *Scuola Normale Superiore, Pisa, Italy*
- ^u *Università degli Studi di Milano, Milano, Italy*
- [†] *Deceased*